J Biomol NMR (2014) 60:99–107
DOI 10.1007/s10858-014-9857-8

ARTICLE

Measuring hydrogen exchange in proteins by selective water saturation in ^{1}H–^{15}N SOFAST/BEST-type experiments: advantages and limitations

Enrico Rennella · Zsofia Solyom · Bernhard Brutscher

Received: 25 June 2014 / Accepted: 22 August 2014 / Published online: 31 August 2014

Abstract HET^{ex}-SOFAST NMR (Schanda et al. in J Biomol NMR 33:199–211, 2006) has been proposed some years ago as a fast and sensitive method for semi-quantitative measurement of site-specific amide-water hydrogen exchange effects along the backbone of proteins. Here we extend this concept to BEST readout sequences that provide a better resolution at the expense of some loss in sensitivity. We discuss the theoretical background and implementation of the experiment, and demonstrate its performance for an intrinsically disordered protein, 2 well folded globular proteins, and a transiently populated folding intermediate state. We also provide a critical evaluation of the level of accuracy that can be obtained when extracting quantitative exchange rates from HET^{ex} NMR measurements.

Keywords BEST · SOFAST · Fast NMR · Hydrogen exchange · Protein · Folding · Unfolding · Compactness · α-synuclein

Electronic supplementary material The online version of this article (doi:10.1007/s10858-014-9857-8) contains supplementary material, which is available to authorized users.

E. Rennella · Z. Solyom · B. Brutscher (✉)
Institut de Biologie Structurale, Université Grenoble 1, 71 avenue des Martyrs, 38044 Grenoble Cedex 9, France
e-mail: bernhard.brutscher@ibs.fr

E. Rennella · Z. Solyom · B. Brutscher
Commissariat à l'Energie Atomique et aux Energies Alternatives (CEA), Grenoble, France

E. Rennella · Z. Solyom · B. Brutscher
Centre National de Recherche Scientifique (CNRS), Grenoble, France

Introduction

Hydrogen exchange measurements of amide protons with solvent protons provide useful information on local structural and dynamic properties of proteins, e.g. solvent accessibility, hydrogen bond strength, local and global unfolding events. Such measurements also allow mapping protein–ligand and protein–protein interactions via a change in the apparent solvent accessibility of amide protons at the protein surface. NMR spectroscopy is a well-established technique to measure hydrogen exchange rates in proteins in a site-resolved manner (Dempsey 2001; Englander and Kallenbach 1983). In the most widely used experimental setup, the protonated protein is quickly dissolved in D_2O, and the disappearance of amide proton NMR signals as a consequence of H/D exchange processes is followed in real-time by recording a series of ^{1}H–^{15}N correlation spectra (Wagner and Wüthrich 1982). Using fast acquisition techniques, such H/D exchange methods are suitable for measuring exchange rates up to $k_{ex} < 0.1\ s^{-1}$ (Gal et al. 2007; Schanda et al. 2007). To detect and quantify faster exchange processes, a variety of conceptually similar magnetization transfer techniques have been proposed (Fan et al. 2011; Gemmecker et al. 1993; Grzesiek and Bax 1993; Hwang et al. 1998; Mori et al. 1994; Wider et al. 1996). The basic idea of these methods is to selectively excite (or frequency-label) the water proton spins, and then observe the transfer of magnetization to amide protons, by repeating the experiment for increasing transfer times. Magnetization transfer techniques provide access to exchange rates in the range $1\ s^{-1} < k_{ex} < 100\ s^{-1}$. The upper limit of quantification of exchange rates is determined by the signal-to-noise ratio of the corresponding exchange line-broadened NMR signals, while the lower limit is imposed by longitudinal relaxation.

Even faster exchange, resulting in unobservable proton resonances, can be quantified by measuring the exchange-induced modulation of ^{15}N-^{1}H scalar couplings (Segawa et al. 2008). The CLEANEX-PM transfer sequence (Hwang et al. 1998) is arguably the current gold standard for measuring fast exchange rates of NMR-visible amide protons in globular proteins, as it suppresses to a large extent direct and exchange-relayed NOE contributions that otherwise introduce systematic errors in the measured exchange rates. A different method of chemical exchange spectroscopy is SOLEXSY (Chevelkov et al. 2010) where magnetization transfer from a protonated to deuterated ^{15}N, and vice versa is measured. While SOLEXSY is not affected by additional magnetization transfer pathways, this method suffers from relatively low intrinsic experimental sensitivity. A few years ago, we introduced yet another technique, called HET^{ex}-SOFAST NMR (Schanda et al. 2006), that provides a semi-quantitative measure of fast hydrogen exchange rates along the polypeptide chain of proteins. In this experiment, the effect of saturating the water protons on the longitudinal relaxation rates (R_1) of amide protons during the recycle (inter-scan) delay is exploited as a measure of the hydrogen exchange efficiency. The main advantages of HET^{ex}-SOFAST with respect to other magnetization transfer techniques are high experimental sensitivity and short overall acquisition times. In the present manuscript, we discuss the experimental and theoretical background of HET^{ex}-SOFAST, and demonstrate that the same idea can be easily extended to BEST-type experiments (HET^{ex}-BEST). In addition, we evaluate experimentally the range of exchange rates accessible to this technique, and the level of accuracy that can be obtained from their quantification.

Theoretical background

If we assume for simplicity a spin system consisting of a labile (exchange-prone) amide proton (A) from the protein under investigation, and a second proton (W) from the bulk water, the time evolution of spin polarization is described by the following set of 1st order differential Bloch-McConnell equations:

$$\frac{d}{dt}\begin{pmatrix} W_z(t) \\ A_z(t) \end{pmatrix} = -\begin{pmatrix} R_1^W & 0 \\ 0 & R_1^A \end{pmatrix}\begin{pmatrix} W_z(t) - W_z^{eq} \\ A_z(t) - A_z^{eq} \end{pmatrix} + \begin{pmatrix} 0 & 0 \\ k_{ex} & -k_{ex} \end{pmatrix}\begin{pmatrix} W_z(t) \\ A_z(t) \end{pmatrix} \quad (1)$$

with R_1^W and R_1^A the longitudinal relaxation rates of water and amide protons, and k_{ex} the hydrogen exchange rate. Equation (1) assumes that the bulk water polarization is not significantly changed by hydrogen exchange with the protein. We now consider two different scenarios that are relevant for the HET^{ex}-SOFAST/BEST experiment described below: (1) in the *reference experiment*, the amide polarization at time $t = 0$ equals $A_z^{ref}(0) = 0$, and the water polarization is close to equilibrium ($W_z^{ref}(t) \approx W_z^{eq}$) throughout the experiment. (2) In the saturation experiment, the amide polarization at time $t = 0$ also equals $A_z^{sat}(0) = 0$, and the water polarization $W_z^{sat}(t) = 0$ for all relaxation times. Under these conditions, solving Eq. (1) yields the following solutions for the evolution of amide proton polarization A_z^{ref} and A_z^{sat} as a function of a relaxation delay d_{relax}:

$$A_z^{ref}(d_{relax}) = A_z^{eq}\frac{R_1^A + k_{ex}W_z^{ref}(d_{relax})}{R_1^A + k_{ex}}\left[1 - \exp\left\{-\left(R_1^A + k_{ex}\right)d_{relax}\right\}\right] \quad (2)$$

$$A_z^{sat}(d_{relax}) = A_z^{eq}\frac{R_1^A}{R_1^A + k_{ex}}\left[1 - \exp\left\{-\left(R_1^A + k_{ex}\right)d_{relax}\right\}\right] \quad (3)$$

In order to determine reliable exchange rates k_{ex} (as well as R_1^A and A_z^{eq}) from Eqs. (2) and (3), measurements of $A_z^{ref}(d_{relax})$, $A_z^{ref}(d_{relax})$, and $W^{ref}(d_{relax})$ need to be performed at a minimum of 2 different relaxation times d_{relax}. Alternatively, if such data are only available for a single relaxation time, we still can compute the following expression, yielding a measure of k_{ex}/R_1^A:

$$HET^{ex}ratio = \frac{\left(A_z^{ref}(d_{relax})/A_z^{sat}(d_{relax}) - 1\right)}{W_z^{ref}(d_{relax})} = \frac{k_{ex}}{R_1^A} \quad (4)$$

In a real protein, dipolar interactions with other protons close in space that exchange (or not) with water protons will offer additional relaxation pathways via NOE and exchange-relayed NOE effects that result in more complex spin dynamics that are not accounted for by a simple fit of the measured data to Eqs. (2) and (3).

The HET^{ex}-SOFAST/BEST experiment

In order to evaluate the effect of hydrogen exchange on the apparent longitudinal relaxation rates of amide protons along the protein backbone, 2 complementary 2D ^{1}H–^{15}N correlation spectra need to be recorded: (1) a reference spectrum, and (2) a water-saturated spectrum. For the reference spectrum, an experiment is required that yields minimal perturbation of water proton polarization, in order to allow for fast repetition of the pulse sequence. This is achieved by SOFAST-HMQC (Schanda and Brutscher 2005; Schanda et al. 2005), BEST-HSQC (Lescop et al. 2007) or BEST-TROSY (Favier and Brutscher 2011) pulse schemes that affect only little the water ^{1}H polarization,

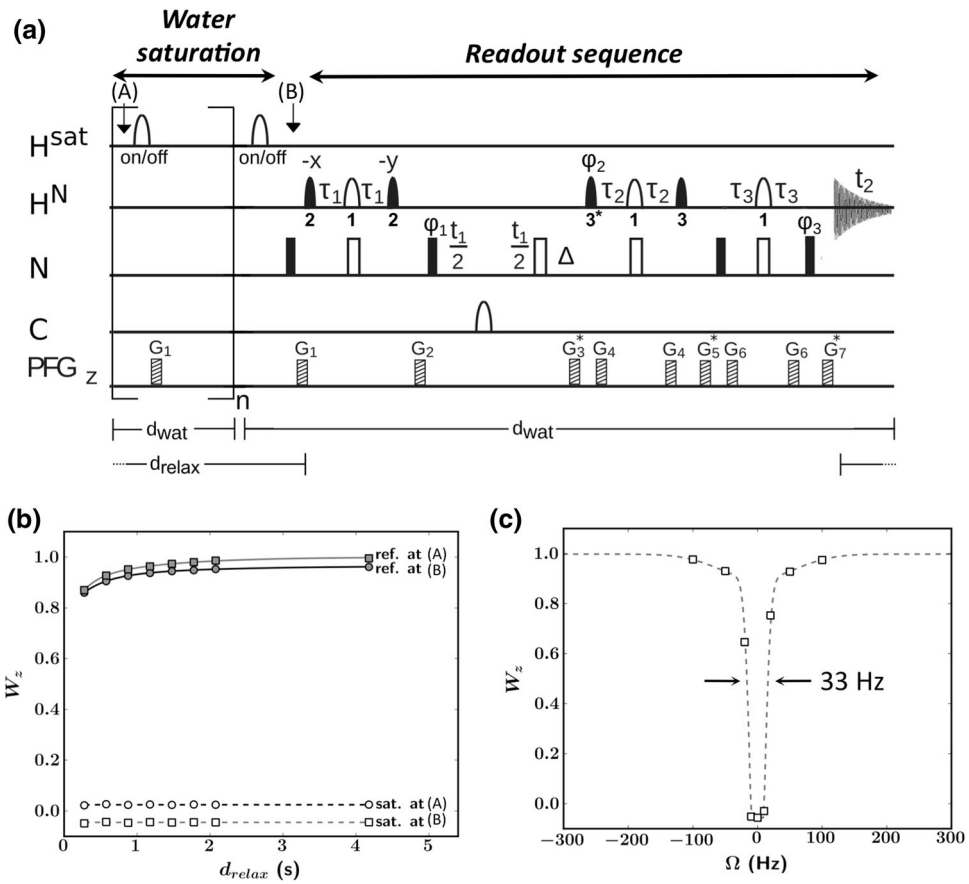

Fig. 1 **a** Pulse sequence of HET^{ex}-BEST-TROSY experiment (the Bruker code is provided in the Supporting Information). The pulse sequence is basically a BEST-TROSY experiment (Favier and Brutscher 2011) to read-out the effect of water saturation on the amide ^{1}H relaxation. Note that only the ^{1}H pathway is detected, while the ^{15}N pathway is removed (by a 90° ^{15}N pulse followed by a pulsed field gradient). For hydrogen exchange measurements, 2D ^{1}H–^{15}N spectra are recorded with (saturation spectrum) and without (reference spectrum) the water saturation scheme applied during the relaxation delay d_{relax}. Water saturation is achieved by a series of on-resonance ISNOB-5 pulses (pulse duration of 150 ms at 600 MHz) followed by a pulsed field gradient to suppress radiation damping. The repetition time d_{wat} is typically set to the duration of the BEST-TROSY readout sequence (including the acquisition period and the length of a single ISNOB-5 pulse). Filled and open pulse symbols indicate 90° and 180° pulses, respectively. Unless indicated, all pulses are applied with phase x. The following pulse shapes are used for H^{N}: [1] REBURP (Geen and Freeman 1991), [2] PC9 (Kupce and Freeman 1994), and [3] E-BURP2 (Geen and Freeman 1991). A *star* indicates a flip-back pulse obtained by time inversion of the excitation pulse shape. H^{N} pulses are typically centred at 8.5 ppm, covering a bandwidth of 4.0 ppm. The transfer delays are adjusted to $\tau_1 = 1/(4J_{NH}) - 0.5\delta_1\_0.5\ \ \delta_2$, $\tau_2 = 0.8/(4J_{NH}) - 0.5\ \ \delta_3\_0.5\ \ \delta_1$, $\tau_3 = 1/(4J_{NH}) - 0.5\ \delta_1$, with $1/(4J_{NH}) \approx 2.7$ ms. The delays δ_1, δ_2 and δ_3 correspond to the ^{1}H pulse lengths of the REBURP, PC9, and E-BURP2, respectively. A 2-step phase cycle is used: $\varphi_1 = x,-x$; $\varphi_2 = y$; $\varphi_3 = y$ For echo/antiecho-type quadrature detection in t_1, 2 data sets are recorded with the relative gradient strengths of G3, G5 and G7 set to (−8: 2: 3.013) and (−7: 3: 1.987), respectively, together with a 180° phase shift of φ_2 and φ_3. **b** Normalized water polarization measured in the reference and saturation experiments as a function of the relaxation delay d_{relax}. For these measurements a small-angle (~1°) read-out pulse, preceded by a strong pulsed field gradient pulse, is inserted at time points (**a**) or (**b**) in the pulse sequence. **c** Normalized water polarization measured at time point (**b**) of the pulse sequence as a function of the offset of the H^{sat} pulses from the water resonance frequency

even under fast-pulsing conditions. Note that even a slight saturation (5–10 %) of the water polarization by the pulse sequence has a dramatic affect on the steady-state water polarization due to the long water T_1 of several seconds ($R_1^w = 0.3\ s^{-1}$ at 25 °C). For the water-saturation experiment, the same ^{1}H–^{15}N spectrum is recorded but with an additional train of regularly spaced selective ^{1}H 180° pulses applied at the water ^{1}H resonance during the recycle delay between subsequent scans. The pulse sequence for HET^{ex}-BEST-TROSY is shown in Fig. 1a. The BEST-TROSY sequence has been chosen here, because it yields highest spectral resolution, especially at high magnetic fields, at the expense of somewhat reduced sensitivity with respect to SOFAST-HMQC (Favier and Brutscher 2011). In order to measure the effect of the pulse sequence on the water polarization, we have added a small-angle (~1°) read-out pulse at positions (a) or (b) in the pulse sequence. The result of such measurements, shown in Fig. 1b,

indicates that the water ^{1}H polarization stays at more than 80 % of its equilibrium value, even for relaxation delays as short as 200 ms.

A critical point for this experiment is the choice of the selective ^{1}H pulses to achieve good water saturation over a narrow bandwidth, independent of the relaxation delay. In addition, if a high-Q cryogenically cooled probe is used for the experiment, the effective B_1 field needs to be stronger than the B_1 field induced by radiation damping (Krishnan and Murali 2013; Shishmarev and Otting 2011) in order to achieve proper inversion of the water ^{1}H polarization by the pulse. As an example, a Gaussian pulse shape of 100 ms length at 600 MHz ^{1}H frequency, as used in our original HET^{ex}-SOFAST experiment (Schanda et al. 2006) does not result in more than 50 % saturation of the water on a high-Q probe under steady-state conditions. Significantly shorter pulse lengths (< 40 ms) with higher B_1 fields are required to achieve efficient water saturation, that will have a strong negative impact on the selectivity of the saturation scheme. We therefore have tested different pulse shapes and pulse lengths, and we obtained good results with an ISNOB-5 pulse (Kupce et al. 1995) of about 150 ms duration. The saturation scheme consists in a repetitive series of a water-selective 180° pulse followed by a relaxation delay (equal to the duration of the readout pulse sequence). The shortest possible relaxation delay therefore corresponds to the length of the selective pulse. After about 40 repetitions of this saturation scheme (dummy scans), steady-state conditions are reached with a residual water ^{1}H polarization close to zero (Fig. 1b). The experimentally determined offset-dependence of water saturation is shown in Fig. 1c, indicating that only protons resonating in close proximity of the water ^{1}H ($\pm$ 20 Hz) are significantly affected by this pulse scheme.

Application to an intrinsically disordered protein

A first application of HET^{ex}-BEST-TROSY to the intrinsically disordered 140-residue protein (IDP) α-synuclein (pH 7.4, 5 °C) is shown in Fig. 2. For IDPs, hydrogen-exchange measurements may be useful probes to identify

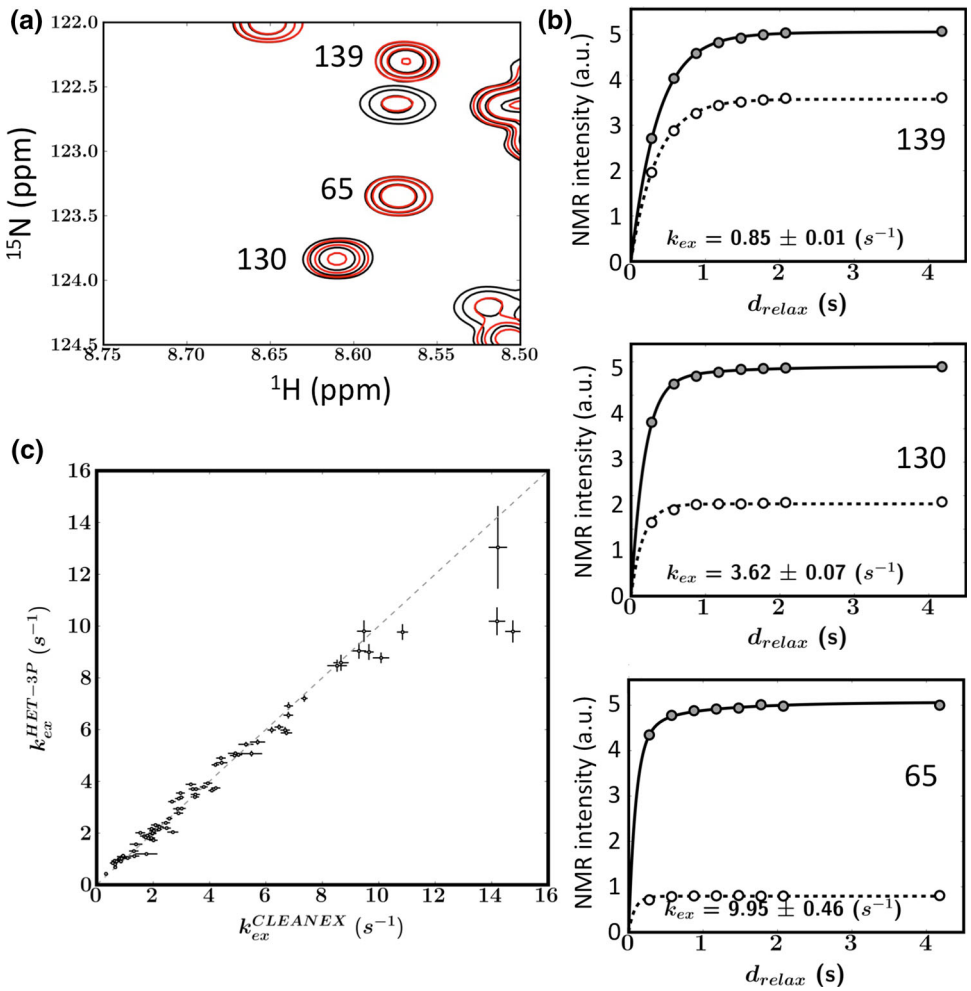

Fig. 2 Hydrogen exchange measurements for amide protons in α-synuclein. **a** Small spectral region of the ^{1}H–^{15}N HET^{ex}-BEST-TROSY reference (*black*) and saturation (*red*) spectra recorded for $d_{relax} = 270$ ms. **b** Intensity *buildup curves* measured for different residues, annotated in (**a**), in a series of reference spectra (*straight lines*) and saturation spectra (*dashed lines*), recorded for different relaxation delays. **c** Correlation plot of exchange rates k_{ex} obtained from a 3-point data fit to Eqs. (2) and (3) and from CLEANEX-PM measurements. Data are shown for all α-synuclein residues for which a resolved ^{1}H–^{15}N correlation peak was detected in the NMR spectra. *Error bars* were obtained from Monte Carlo simulations based on the spectral noise level

partially structured peptide segments, and to evaluate changes in solvent accessibility under different sample conditions, or upon binding to a molecular partner (Croke et al. 2008; Crowhurst et al. 2002; Csizmok et al. 2008). HET^{ex}-BEST-TROSY (reference and saturation) spectra have been measured for relaxation delays d_{relax} in the range 200 ms–4.2 s. The relaxation curves for 3 representative residues (Fig. 2a) are plotted in Fig. 2b. These data nicely illustrate the differences observed in the relaxation behavior of amide protons along the backbone of α-synuclein under water-saturating conditions. The fast amide ^{1}H relaxation observed for fast exchanging amide sites can also be exploited to enhance the signal intensity of the corresponding correlation peaks in SOFAST- and BEST-type experiments (Gil et al. 2013; Yao et al. 2011). In order to extract quantitative exchange rates, these relaxation curves were fitted to Eqs. (2) and (3), using either all measured time points, or a minimal data set (3 points) consisting in 2 reference spectra "together with measurement of the water polarization $W^{ref}(d_{relax})$", measured at 2 relaxation times (d_{relax} = 200 and 500 ms), and one saturation spectrum obtained for a single relaxation delay of d_{relax} = 200 ms. As both fits yield very similar results (see figure S1 of the Supporting Information), only exchange rates obtained from the 3-point fits will be discussed in the following.

In order to evaluate the accuracy of the exchange rates extracted from the HET^{ex}-BEST-TROSY data, we also have performed CLEANEX-PM measurements (Hwang et al. 1998) on the same sample. Details on the experimental setup are provided in figure S2 of the Supporting Information. As shown in Fig. 2c, the CLEANEX-PM "reference" exchange rates correlate well with the rates extracted from HET^{ex}-BEST-TROSY in the range 0.1 $s^{-1} < k_{ex} < 10$ s^{-1}. Higher exchange rates cannot be quantified accurately from HET^{ex}-BEST-TROSY data, as the relaxation curves under water-saturation conditions become flat, in other words the plateau peak intensity has been reached within the shortest relaxation time (d_{relax} = 200 ms). However, it is worth noting that the CLEANEX-PM sequence has also a limited accuracy in this regime, as for peptide segments that undergo fast time-scale local motions the conditions underlying the suppression scheme of NOE and ROE effects are no longer satisfied.

In conclusion of this part, HET^{ex}-BEST-TROSY yields accurate exchange rate measurements for highly dynamic proteins or protein segments over a range of about 2 orders of magnitude (0.1 $s^{-1} < k_{ex} < 10$ s^{-1}), by measuring a minimal data set of 3 ^{1}H–^{15}N correlation spectra, and fitting the measured data to the analytical solutions of the Bloch-McConnell equations for an isolated 2-spin system as given by Eqs. (2) and (3). The main advantage of this approach is that the overall data acquisition time for HET^{ex}-BEST-TROSY was only 40 min, while CLEANEX-PM required 24 h of data collection on the same NMR spectrometer.

Application to globular proteins

The same strategy for evaluating the performance of HET^{ex}-BEST-TROSY, as outlined above for α-synuclein, has been applied to 2 small well-folded proteins: (1) the 76-residue *human* ubiquitin (pH 6.4, 20 °C), and (2) the 70-residue *E. coli* heat-shock protein CspA (pH 7.7, 15 °C). Correlation plots of exchange rates extracted from HET^{ex}-BEST-TROSY and CLEANEX-PM data are shown in Fig. 3a (ubiquitin), d (CspA). The majority of amide protons in these globular proteins are involved in hydrogen-bonded secondary structural elements, and thus exhibits relatively slow solvent exchange with k_{ex} rates of < 2 s^{-1}. Comparison with the rates obtained from CLEANEX-PM shows that there is almost no correlation for amides in the structured parts of the proteins, while the correlation is quite good for the few residues in mobile loop regions that exhibit faster exchange, $k_{ex} > 2$ s^{-1}. The lack of correlation in the structured protein regions is explained by the fact that dipolar (NOE) interactions between the amide proton and nearby labile (O–H, N–H, $N–H_2$) protons, or H^{α} protons resonating close to the water frequency, contribute up to 2 s^{-1} to the apparent exchange rates in HET^{ex}-BEST-TROSY, while they are suppressed to a large extent in CLEANEX-PM. A particularly striking example is residue S27 of CspA that shows the largest discrepancy between the HET^{ex}-BEST-TROSY and CLEANEX-PM data. A zoom into the structural region surrounding S27 (see figure S3 of the Supporting Information) shows that the amide proton is only at a distance of 2.2 Å from its own side-chain O–H. The apparent k_{ex} = 1.7 s^{-1} extracted from HET^{ex}-BEST-TROSY is thus due to an exchange-relayed NOE effect with this side chain proton, and not to a direct hydrogen exchange of the amide proton with water. If the exchange process is in the so-called EX2 regime, where the folding (closing) rate is much faster than the intrinsic chemical exchange rate, the accuracy of the measured exchange rates can be increased by repeating the HET^{ex}-BEST-TROSY experiment for different pH values, as proposed by Bax and coworkers (Fitzkee et al. 2011). However, due to the limited range of exchange rates accessible by this technique, only small pH variations should be used in practice.

As an alternative to the extraction of quantitative exchange rates from HET^{ex}-BEST-TROSY data measured for multiple relaxation delays, we can compute the HET^{ex}ratio, introduced in Eq. 4, from a pair of HET^{ex}-BEST-TROSY spectra recorded for a single relaxation

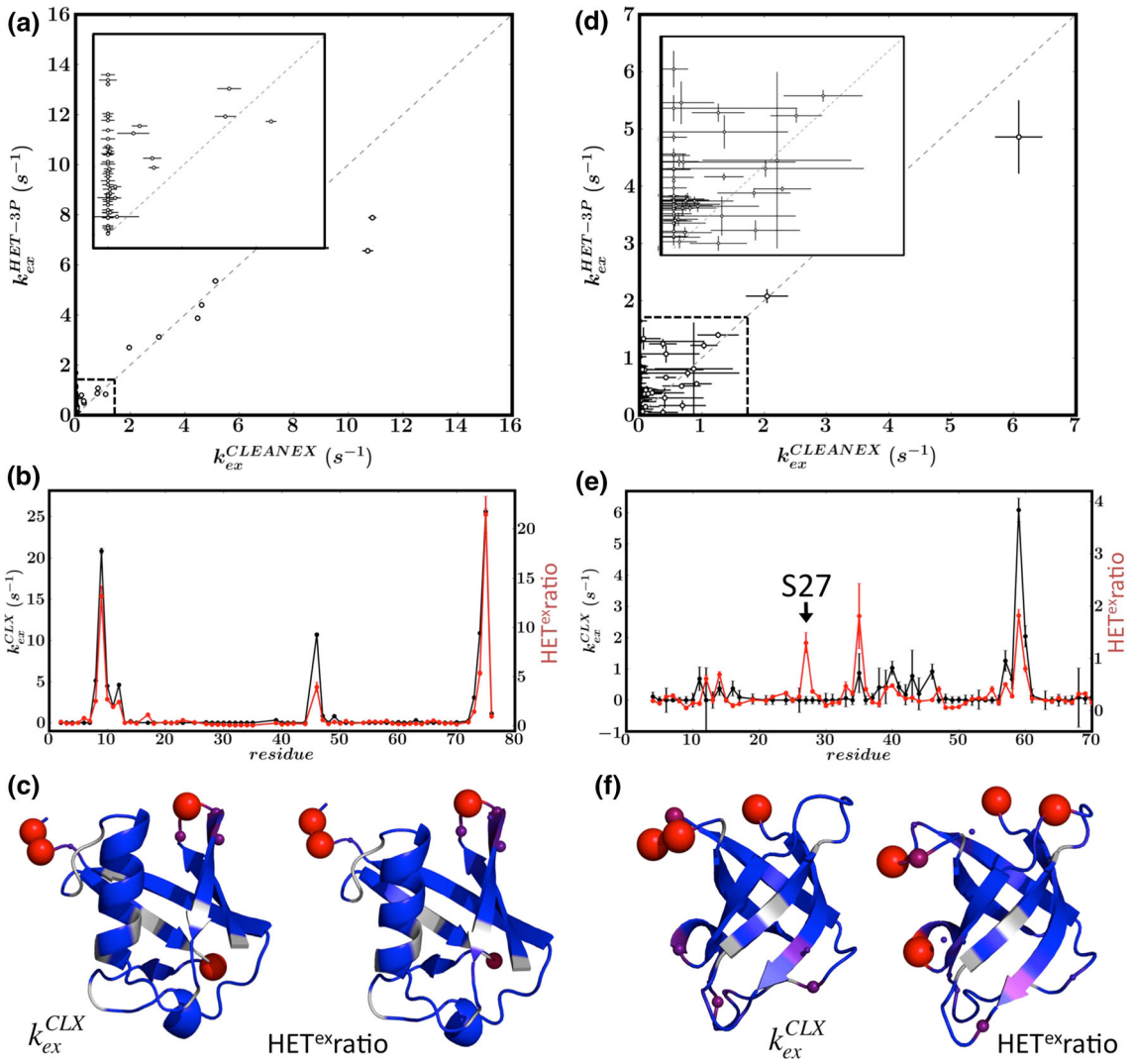

Fig. 3 Hydrogen exchange measurements for ubiquitin (*left panel*) and CspA (*right panel*). **a** and **d** Correlation of exchange rates k_{ex} extracted from HET^{ex}-BEST-TROSY and CLEANEX-PM data. CLEANEX-PM k_{ex} rates (*black lines*) and *HET^{ex}ratios* (*red lines*) are plotted as a function of peptide sequence in (**b**) and (**e**), and color-coded on the crystal structures of ubiquitin (PDB 1UBQ) in (**c**) and CspA (PDB 1MJC) in (**f**). *A larger ball size* indicates faster exchange; while *gray* regions indicate the absence of NMR data, either because of spectral overlap or due to missing assignment. *Error bars* for k_{ex} rates were obtained from Monte Carlo simulations based on the measured spectral noise level, while *error bars* for *HET^{ex}ratios* were calculated by error propagation of the spectral noise

delay. If we assume that the longitudinal ^{1}H relaxation rate R_1^A is changing only little from one site to another, a hypothesis that is typically satisfied for well-structured protein regions, HET^{ex}ratios provide a measure of the change in solvent accessibility along the protein backbone. This is shown in Fig. 3b, e for ubiquitin and CspA, respectively. The measured HET^{ex}ratios provide *solvent-exchange profiles* that closely match the results obtained from quantification of exchange rates using CLEANEX-PM. This is especially true if the measured exchange rates fall within the range 0.1 $s^{-1} < k_{ex} < 10$ s^{-1} (example of ubiquitin), where the HET^{ex}-BEST-TROSY approach is most sensitive. For both proteins, the measured HET^{ex}-ratios allow to differentiate between solvent-exposed and hydrogen-bonded amide sites as illustrated by the structural drawings in Fig. 3c, f.

We can conclude that HET^{ex}-BEST-TROSY, if performed for a single pH value, does not provide a valuable tool for accurate quantification of exchange rates in well-structured hydrogen-bonded parts of proteins, but it provides a fast and sensitive technique for the characterization of local structural compactness and water accessibility in globular proteins, as already outlined in our previous work (Schanda et al. 2006).

Application to a transiently populated protein folding intermediate

The HET^{ex} SOFAST/BEST technique is particularly interesting for applications to short-lived or transiently populated protein states, for which fast and sensitive NMR methods are mandatory. This is demonstrated here for the example of the amyloidogenic protein β2-microglobulin (B2M). It has been shown previously that during the refolding process from a highly unstructured to the well-structured native state, a folding intermediate (I-state) accumulates that is characterized by a non-native *trans* peptide bond between residues His^{31} and Pro^{32} (Kameda et al. 2005). This I-state is thought to be involved in the

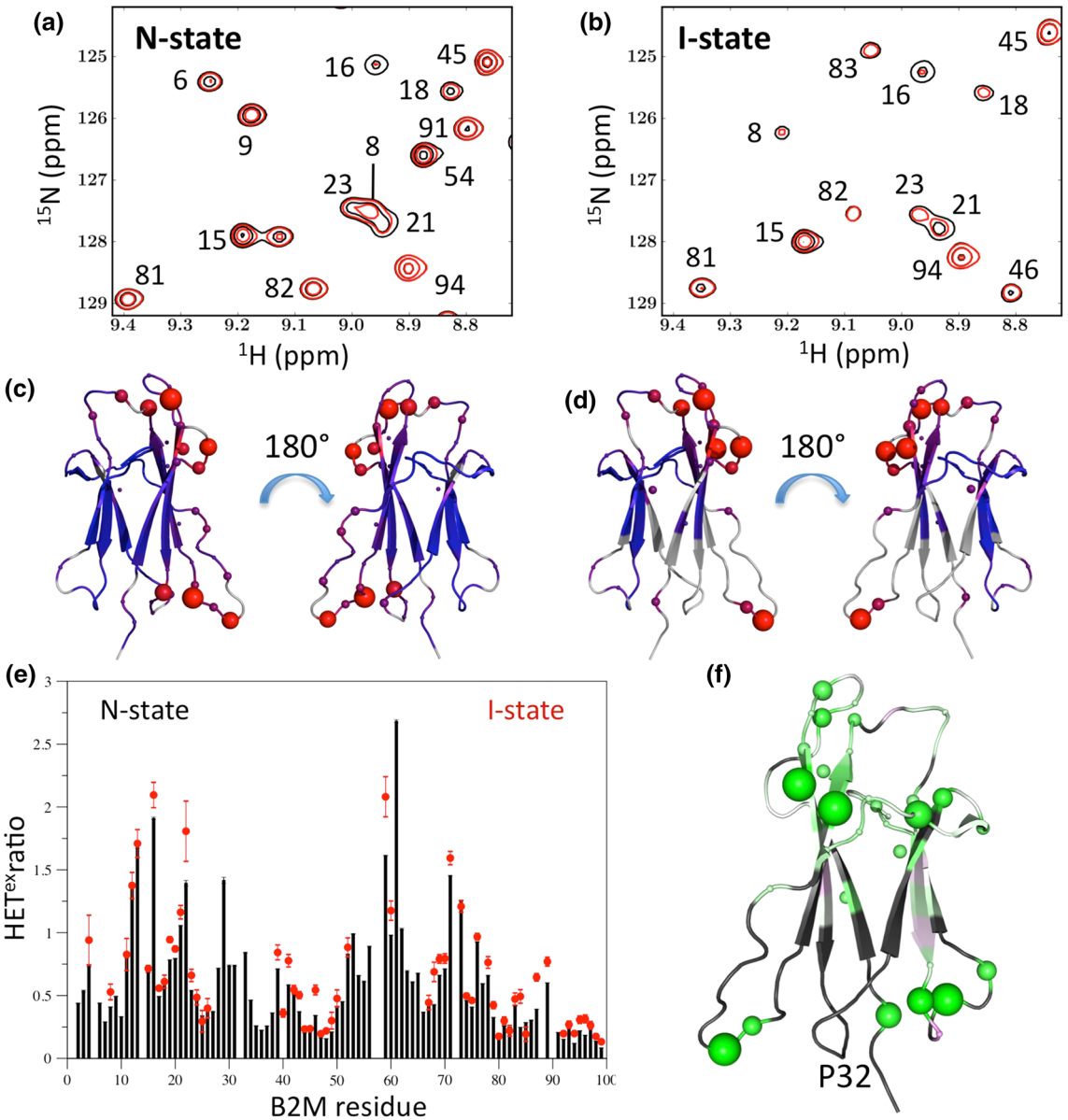

Fig. 4 Real-time hydrogen exchange measurements during the refolding of the amyloidogenic protein β2-microglobulin (B2M). Spectral regions of the ^{1}H–^{15}N HET^{ex}-BEST-TROSY reference (*black*) and saturation (*red*) spectra recorded for the N-state (**a**) and I-state (**b**) of B2M. CLEANEX-PM k_{ex} rates and *HET^{ex}ratios* measured for the N-state (**c**) and I-state (**d**) color-coded on the solution structure of B2M (PDB 2XKS). In **e** the same data are plotted as a function of the peptide sequence for the N-state (*black bars*) and I-state (*red circles*). *Error bars* for *HET^{ex}ratios* were calculated by error propagation of the spectral noise. **f** Differences between *HET^{ex}ratios* measured for the N- and I-states color-coded on the crystal structure of B2M. *A larger ball size* indicates faster exchange; while *gray* regions indicate the absence of NMR data, either because of spectral overlap or due to missing assignment

onset of amyloid fibril formation. Therefore obtaining atomic-resolution information on the I-state is of fundamental importance for a better understanding of the process of amyloidogenesis. Recently, using real-time multidimensional NMR, we have obtained sequential resonance assignments, as well as some information on the conformational dynamics in the I-state (Rennella et al. 2012). We could also demonstrate that the I-state binds to the hydrophobic dye ANS, while no such interaction is observed for the protein in its native state (Rennella et al. 2013). Under the chosen temperature of 15 °C, the I-state has a half-life time of ~20 min, meaning that the maximum available experimental time for an NMR experiment of the I-state is about 40 min. Figure 4a, b show a small region of HET^{ex}-BEST-TROSY spectra recorded for the N-state, and the I-state of B2M, reconstructed from real-time NMR data. The spectral quality is sufficient to calculate HET^{ex}ratios for a large number of amide protons in the I-state. The measured HET^{ex}ratios are color-coded on the B2M structure in Fig. 4c (N-state), d (I-state), and plotted as a function of the protein sequence in Fig. 4e. A first conclusion from these data is that HET^{ex}-BEST-TROSY yields meaningful information on the solvent accessibility along the peptide chain of short-lived protein folding intermediates. Overall, the solvent-exchange profiles measured for the N- and I-states are very similar. Interestingly, however, a closer inspection of the rate differences between I- and N-states indicates a higher apparent solvent accessibility in the I-state loop regions at both sides of the protein (see Fig. 4f), while the hydrogen-bonding in the β-sheet region seems to be largely identical in the 2 states, in agreement with ^{13}C secondary chemical shift data reported previously (Rennella et al. 2012). An alternative interpretation of the observed differences between the N and I states would be a more compact overall conformation of the folding intermediate that may result in an increase of the NOE contribution to the measured HET^{ex}ratios.

Conclusions

We have demonstrated here that the measurement of amide ^{1}H polarization recovery rates under water saturating and non-saturating conditions provides a fast measure of hydrogen exchange processes along the backbone of ^{15}N-labeled proteins. SOFAST- and BEST-type readout sequences are ideally suited for HET^{ex} NMR as they minimally perturb the water ^{1}H polarization, thus allowing for high repetition rates (fast-pulsing), short overall acquisition times, and high experimental sensitivity. Typically, in case of abundant sensitivity, a full HET^{ex}–BEST data set can be recorded in a few minutes (and even less in case of HET^{ex}–SOFAST). We have presented two different approaches of data analysis: (1) Residue-specific HET^{ex} ratios can be computed from a pair of 2D NMR spectra recorded for a short relaxation delay, providing a semi-quantitative measure of the relative exchange efficiency along the peptide chain. This approach is most suitable for globular proteins or heterogeneous proteins with structured and unstructured parts, and it provides an efficient and fast method for distinguishing residues in structured and highly mobile protein regions. (2) If a second reference spectrum recorded for a longer relaxation delay is available, this allows extracting quantitative exchange rate constants, as long as Eq. (1) is valid. We have shown that for IDPs or highly disordered protein fragments, this approach yields accurate exchange rates in the range $0.1\ s^{-1} < k_{ex} < 10\ s^{-1}$, and thus provides an attractive alternative to CLEANEX-PM or other magnetization-transfer techniques, yielding similar results in much shorter experimental time. Finally, the potentially most interesting application of HET^{ex} NMR is the investigation of fast hydrogen exchange processes in short-lived protein states, as illustrated here for a folding intermediate of the amyloidogenic human protein β2-microglobulin that can only be studied by real-time NMR methods, requiring fast multidimensional data acquisition. HET^{ex} NMR adds a new probe of structural information for such transiently populated protein states. Similarly, HET^{ex} NMR may prove useful for investigating protein stability inside living cells or in cell extracts (Smith et al. 2013) where protein leakage and protein degradation limits the available measurement time for a single sample.

Acknowledgments We thank Isabel Ayala and Karine Giandoreggio for expert protein sample preparation, and we acknowledge support from ANR grant Blanc-InterII-SIMI7-2011 (RNAfolding). This work used the NMR and isotope labeling platforms of the Grenoble Instruct centre (ISBG; UMS 3518 CNRS-CEA-UJF-EMBL) with support from FRISBI (ANR-10-INSB-05-02) and GRAL (ANR-10-LABX-49-01) within the Grenoble Partnership for Structural Biology (PSB).

References

Chevelkov V, Xue Y, Rao DK, Forman-Kay JD, Skrynnikov NR (2010) 15 N H/D-SOLEXSY experiment for accurate measurement of amide solvent exchange rates: application to denatured drkN SH3. J Biomol NMR 46:227–244

Croke RL, Sallum CO, Watson E, Watt ED, Alexandrescu AT (2008) Hydrogen exchange of monomeric alpha-synuclein shows unfolded structure persists at physiological temperature and is independent of molecular crowding in Escherichia coli. Protein Sci 17:1434–1445

Crowhurst KA, Tollinger M, Forman-Kay JD (2002) Cooperative Interactions and a Non-native Buried Trp in the Unfolded State of an SH3 Domain. J Mol Biol 322:163–178

Csizmok V, Felli IC, Tompa P, Banci L, Bertini I (2008) Structural and dynamic characterization of intrinsically disordered human securin by NMR spectroscopy. J Am Chem Soc 130:16873–16879

Dempsey CE (2001) Hydrogen exchange in peptides and proteins using NMR spectroscopy. Prog in NMR Spectrosc 39:135–170

Englander SW, Kallenbach NR (1983) Hydrogen exchange and structural dynamics of proteins and nucleic acids. Q Rev Biophys 16:521–655

Fan J-S, Lim J, Yu B, Yang D (2011) Measurement of amide hydrogen exchange rates with the use of radiation damping. J Biomol NMR 51:151–162

Favier A, Brutscher B (2011) Recovering lost magnetization: polarization enhancement in biomolecular NMR. J Biomol NMR 49:9–15

Fitzkee NC, Da Torchia, Bax A (2011) Measuring rapid hydrogen exchange in the homodimeric 36 kDa HIV-1 integrase catalytic core domain. Protein Sci 20:500–512

Gal M, Schanda P, Brutscher B, Frydman L (2007) UltraSOFAST HMQC NMR and the repetitive acquisition of 2D protein spectra at Hz rates. J Am Chem Soc 129:1372–1377

Geen H, Freeman R (1991) Band-selective radiofrequency pulses. J Magn Reson 93:93–141

Gemmecker G, Jahnke W, Kessler H (1993) Measurement of fast proton exchange rates in isotopically labeled compounds. J Am Chem Soc 115:11620–11621

Gil S, Hošek T, Solyom Z, Kümmerle R, Brutscher B, Pierattelli R, Felli IC (2013) NMR Spectroscopic Studies of Intrinsically Disordered Proteins at Near-Physiological Conditions. Angew Chem Int Ed Engl 52:11808-11812

Grzesiek S, Bax A (1993) Measurement of amide proton-exchange rates and Noes with Water in C-13/N-15-Enriched Calcineurin-B. J Biomol NMR 3:627–638

Hwang TL, van Zijl PC, Mori S (1998) Accurate quantitation of water-amide proton exchange rates using the phase-modulated CLEAN chemical EXchange (CLEANEX-PM) approach with a Fast-HSQC (FHSQC) detection scheme. J Biomol NMR 11:221–226

Kameda A, Hoshino M, Higurashi T, Takahashi S, Naiki H, Goto Y (2005) Nuclear magnetic resonance characterization of the refolding intermediate of beta(2)-microglobulin trapped by non-native prolyl peptide bond. J Mol Biol 348:383–397

Krishnan VV, Murali N (2013) Radiation damping in modern NMR experiments: progress and challenges. Prog in NMR Spectrosc 68:41–57

Kupce E, Freeman R (1994) Wide-Band Excitation with Polychromatic Pulses. J Magn Reson A 108:268–273

Kupce E, Boyd J, Campbell ID (1995) Short selective pulses for biochemical applications. J Magn Reson B 106:300–303

Lescop E, Schanda P, Brutscher B (2007) A set of BEST triple-resonance experiments for time-optimized protein resonance assignment. J Magn Reson 187:163–169

Mori S, O'Neil Johnson M, Berg JM, Van Zijl PCM (1994) Water exchange filter (WEX Filter) for nuclear magnetic resonance studies of macromolecules. J Am Chem Soc 116:11982–11984

Rennella E, Cutuil T, Schanda P, Ayala I, Forge V, Brutscher B (2012) Real-time NMR characterization of structure and dynamics in a transiently populated protein folding intermediate. J Am Chem Soc 134:8066–8069

Rennella E et al (2013) Oligomeric states along the folding pathways of β2-microglobulin: kinetics, thermodynamics, and structure. J Mol Biol 425:2722–2736

Schanda P, Brutscher B (2005) Very fast two-dimensional NMR spectroscopy for real-time investigation of dynamic events in proteins on the time scale of seconds. J Am Chem Soc 127:8014–8015

Schanda P, Kupce E, Brutscher B (2005) SOFAST-HMQC experiments for recording two-dimensional heteronuclear correlation spectra of proteins within a few seconds. J Biomol NMR 33:199–211

Schanda P, Forge V, Brutscher B (2006) HET-SOFAST NMR for fast detection of structural compactness and heterogeneity along polypeptide chains. Magn Reson Chem 44:S177–S184

Schanda P, Forge V, Brutscher B (2007) Protein folding and unfolding studied at atomic resolution by fast two-dimensional NMR spectroscopy. Proc Natl Acad Sci USA 104:11257–11262

Segawa T, Kateb F, Duma L, Bodenhausen G, Pelupessy P (2008) Exchange rate constants of invisible protons in proteins determined by NMR spectroscopy. ChemBioChem 9:537–542

Shishmarev D, Otting G (2011) Radiation damping on cryoprobes. J Magn Reson 213:76–81

Smith AE, Sarkar M, Young GB, Pielak GJ (2013) Amide proton exchange of a dynamic loop in cell extracts. Protein Sci 22:1313–1319

Wagner G, Wüthrich K (1982) Amide Proton Exchange and Surface Conformation Basic Pancreatic Trypsin Inhibitor in Solution. J Mol Biol 160:343–361

Wider G, Riek R, Wüthrich K (1996) Diffusion filters for separation of solvent—protein and protein–protein nuclear overhauser effects (HYDRA). J Am Chem Soc 7863:11629–11634

Yao S, Hinds MG, Murphy JM, Norton RS (2011) Exchange enhanced sensitivity gain for solvent-exchangeable protons in 2D 1H-15 N heteronuclear correlation spectra acquired with band-selective pulses. J Magn Reson 211:243–247